A Chemical Timing Method for Absolute Vibrational Relaxation Rate Constants in the Vibrational Quasi-Continuum Region of S_1 *p*-Difluorobenzene†

Uros S. Tasic and Charles S. Parmenter*

Department of Chemistry, Indiana University, Bloomington, Indiana 47405

Received: December 10, 2003; In Final Form: February 17, 2004

A new method has been developed to measure absolute rate constants for gas-phase collisional vibrational relaxation in high S_1 *p*-difluorobenzene (pDFB) vibrational energy regions where the levels overlap to form a quasi-continuum. The heavily mixed vibrational character of these levels produces $S_1 \rightarrow S_0$ fluorescence without the vibrational structure that is needed to measure rate constants. Following well-studied chemical timing procedures, the addition of large pressures (in the kTorr range) of O_2 to a low pressure pDFB sample yields a structured fluorescence spectrum that proves to be suitable for measurement of absolute rate constants for vibrational relaxation induced by argon added to the pDFB + O_2 mixture. The first application concerns S_1 pDFB with $\epsilon_{vib} = 3700$ cm^{-1} and a high vibrational state density ($\rho_{vib} > 4000$ per cm^{-1}) that creates a quasi-continuum. The absolute rate constant for vibrational energy transfer in Ar collisions from the initially pumped region into the surrounding vibrational field is $k_v^{Ar} = (9.4 \pm 1.5) \times 10^6$ Torr^{-1} s^{-1} = 2.9×10^{-10} cm^3 molecule^{-1} s^{-1}. This rate constant is within the experimental error of rate constants determined previously for three lower levels with $\epsilon_{vib} \geq 2887$ cm^{-1}. The value is roughly 50% of the Lennard-Jones rate constant usually assumed for the vibrational activation/deactivation step of thermal unimolecular reactions. A rate constant analogous to k_v^{Ar} but for O_2 collisions is determined to have approximately the same value as k_v^{Ar}. An approximate intramolecular vibrational redistribution (IVR) rate constant for S_1 pDFB with $\epsilon_{vib} = 3700$ cm^{-1} corresponds to an IVR lifetime in the range of 45−75 ps.

1. Introduction

Collisional vibrational relaxation of large polyatomic molecules (e.g., >10 modes) from high levels of the vibrational manifold has attracted attention for many years, particularly with respect to its role in the vibrational activation/deactivation step of the gas-phase thermal unimolecular reactions.[1−3] A particular focus has been on the average amount of energy (ΔE) transferred in a single collision and on the vibrational energy transfer (VET) probability distribution function $P(E',E)$ for a collision taking a molecule from initial vibrational energy E' to a final energy $E + dE$. The normalization of these quantities to a per collision basis involves an absolute VET rate constant that has neither been measured experimentally nor calculated from theory for any molecule larger than SO_2.[4,5] Instead, the rate constant is usually assumed to be that of an elastic collision operating with a Lennard-Jones intermolecular potential.[6−11]

This report concerns a study designed to give experimental information about the absolute magnitude of such VET rate constants. The constants are those for VET from an initially pumped narrow vibrational region into the surrounding field of vibrational levels. We have previously measured these state-to-field rate constants for various initial levels of S_1 *p*-difluorobenzene (pDFB) in collision with He or Ar.[12,13] Those levels span S_1 vibrational regions from the zero-point level to $\epsilon_{vib} = 3310$ cm^{-1} where the vibrational state density is $\rho_{vib} \approx 2000$ per cm^{-1}. The pattern of rate constants as one climbs the vibrational ladder into regions of large ρ_{vib} provides a way to learn about the Lennard-Jones assumption.[13]

The present work extends the absolute rate constant measurements for Ar collisions to $\epsilon_{vib} = 3700$ cm^{-1}. The seemingly small extension is significant because the higher state density ($\rho_{vib} > 4000$ per cm^{-1}) takes us into a region where the surrounding vibrational field assumes some key characteristics of the fields associated with the activation/deactivation steps of thermal unimolecular reactions. Although our state density is still relatively small, it now becomes high enough to generate even more securely the vibrational quasi-continuum and extensive state mixing typically found in vibrational manifolds encountered in the VET of thermal unimolecular reactions.

The cost of moving to levels above 3310 cm^{-1} in S_1 pDFB is the need to develop a new experimental method for measuring the VET rate constants. The classic experimental approach involves the use of a straightforward optical pump-fluorescence probe.[12−14] An initial S_1 vibrational state is selected by tuned laser pumping, and the vibrational band intensities in the ensuing $S_1 \rightarrow S_0$ fluorescence spectrum are monitored as the molecules are brought increasingly into interactions with an added gas. The collision-free fluorescence time scale provides a clock for establishing absolute rate constants under single-collision conditions.

The spectra in Figure 1 illustrate why the technique fails for levels with $\epsilon_{vib} = 3700$ cm^{-1} and higher. The vibrational bands such as those, for example, in fluorescence from $\epsilon_{vib} = 2068$ cm^{-1} are no longer present in fluorescence after pumping the 3700 cm^{-1} level. The structure associated with single-level emission is replaced by a broad and featureless spectrum. Thus, as is apparent in the collision-free $\epsilon_{vib} = 3700$ cm^{-1} fluorescence spectrum of Figure 1, the experimental handle used to monitor VET is gone. This situation is in fact somewhat ironic. On one

† Part of the special issue "Gerald Small Festschrift".

* Author to whom correspondence should be addressed. FAX: (812) 855-8300. E-mail: parment@indiana.edu.

10.1021/jp031298t CCC: $27.50
Published on Web 05/07/2004

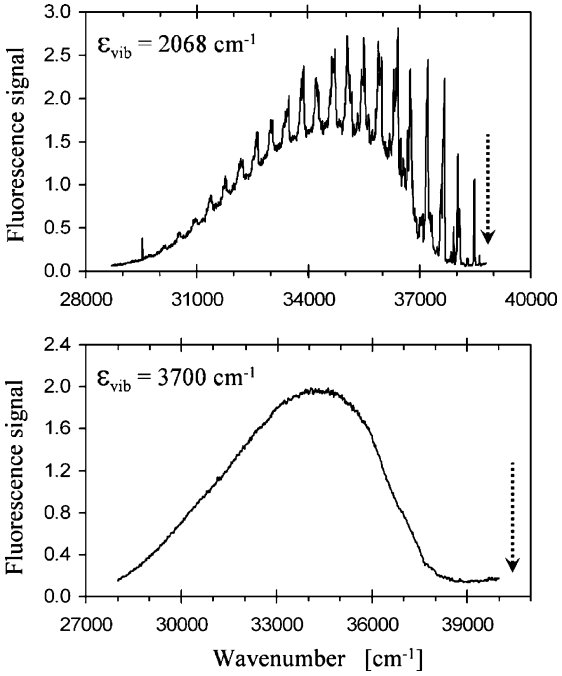

Figure 1. Single vibronic level fluorescence spectrum of collision-free *p*-difluorobenzene (pDFB) pumped to the S_1 level ϵ_{vib} = 2068 cm^{-1} (top) and the level ϵ_{vib} = 3700 cm^{-1} (bottom). The pDFB excitation positions are marked with arrows.

hand, a quasi-continuum of mixed vibrational states is needed to mimic the vibrational characteristics of highly excited reactive molecules. On the other hand, this quasi-continuum leads to the loss of structure in the fluorescence spectrum needed to make the VET measurements.

Earlier studies suggest a resolution of the problem. High pressures (kTorr) of added O_2 transform featureless spectra such as that from ϵ_{vib} = 3700 cm^{-1} to spectra with substantial vibrational structure. The phenomenon is called chemical timing, and it has been extensively studied as an approach to learn about intramolecular vibrational redistribution (IVR) rates in aromatic molecules.[15−21] These studies show that the structure induced by O_2 collisions is that from the pumped S_1 vibrational levels. This finding implies that the recovered structure should provide a means to acquire absolute state-to-field VET rate constants in a manner analogous to the traditional VET experiments.

In this paper, we describe details of this new VET technique by illustrating its application to the ϵ_{vib} = 3700 cm^{-1} level of S_1 pDFB in collision with Ar. As it turns out, the technique requires a sequence of different types of experiments to extract a VET rate constant. The first step involves a quantitative characterization of the O_2 electronic quenching kinetics. Second, vibrational band intensities are measured for various added Ar pressures in the presence of a given O_2 pressure. These intensity measurements are then repeated for a series of fixed O_2 pressures. Finally, the rate constants for IVR and for VET by O_2 itself are measured by chemical-timing procedures worked out previously. Only at the end of this sequence is it possible to extract the absolute magnitude of the desired state-to-field VET rate constant.

We shall refer to experiments that combine chemical timing and classical VET methods as CT-VET studies. Other experiments in this paper use the standard chemical timing method alone to obtain IVR rates, and they are called IVR experiments.

2. Experimental Procedure

Samples of pDFB (99+%) are used without further purification, except for degassing through freeze−pump−thaw cycles. Extra dry grade O_2 and zero grade argon are handled in a grease-free glass vacuum line. Pressures are measured with 10 Torr range and 1000 PSI range MKS Baratron capacitance manometers. In IVR experiments, 0.7 Torr of pDFB is used; in CT-VET experiments, 4−5 Torr of pDFB is used. In both IVR and CT-VET experiments, the O_2 pressure on the order of 10^3−10^4 Torr is sufficiently high to avoid $S_1 + S_0$ pDFB collisions. The gases are contained in a stainless steel T-shaped static fluorescence cell with quartz windows. In the IVR experiments, O_2 gas is incrementally added via a quick leak from a line at a much higher O_2 backing pressure into the cell that contains a constant partial pressure of pDFB. In the CT-VET experiments, argon gas is incrementally added in a similar manner via a quick leak from a line at a much higher argon backing pressure into the cell containing a constant partial pressure of the previously prepared pDFB + O_2 mixture. Long mixing times are required.

A Quanta Ray DCR 1A Nd:YAG laser with a doubling crystal and a PDL-1 dye laser system is used in all experiments. With DCM dye and a wavelength extender, the UV output in the 246.0−247.3 nm region is pulsed at 10 Hz with a pulse duration of ∼6 ns, with an UV energy of ∼40 μJ/pulse and a bandwidth of ∼2 cm^{-1}. The sample is exposed to radiation only during data acquisition to minimize photodecomposition. A small portion of the UV laser beam is diverted into a UV photodiode for monitoring the laser power to correct the fluorescence signal.

Fluorescence is collected at 90° and imaged into a scanning 0.85 m double monochromator (Spex 1401) operated in second order with photomultiplier detection. The detection resolution is set to 20 cm^{-1} for dispersed fluorescence spectrum scans and IVR experiments, to 45 cm^{-1} for CT-VET experiments, and to 100 cm^{-1} for fluorescence excitation scans. The detection wavelength for fluorescence excitation was at the fluorescence maximum near 34 000 cm^{-1}. The signals are acquired and processed by a home-built gated detection system. The detection gate is synchronized to open immediately following the laser pulse and remains open long enough to collect the entire time-integrated fluorescence intensity.

The IVR experiments have a setup and procedure analogous to those performed previously.[17,18] These experiments involve scanning across the entire emission spectrum at various O_2 pressures. The spectrum spans ∼12 000 cm^{-1}. Compared to the width of vibronic bands in a large polyatomic molecule at 300 K, the 20 cm^{-1} detection resolution and 5 cm^{-1} step size are sufficient to distinguish accurately between structured and congested emission without introducing substantial background problems. The frequency integrated fluorescence signal is the sum of photon counts measured at each 5 cm^{-1} step over 2400 steps.

The setup and procedure for standard VET experiments are described elsewhere.[13] Our new CT-VET experiments use similar experimental features, but the principal difference is that now the sample involves a three-component mixture with pDFB + O_2 as the basic component to which argon gas is incrementally added. The fluorescence signal intensity of selected vibrational bands is monitored at each argon pressure increment. Both the pump laser and detection position are fixed during the experiment. The ratio of two signal intensities under different added gas conditions directly represents the ratio of S_1 level populations. For the sake of more secure quantitative data, we monitor independently two different vibrational bands and a baseline position. The detection resolution of 45 cm^{-1} is large enough to ensure simultaneous monitoring of an entire band, eliminating sensitivity to subtle changes in the rotational contour. At the same time, the resolution is not too low to have significant

TABLE 1: Processes that Constitute the Kinetic Model

process	rate constant	description
$B^* \rightarrow S_0 + h\nu_f +$ nonradiative decay of S_1	k_f	electronic decay
$B^* \rightarrow B^{**}$	k_{IVR}	IVR
$O_2 + B^* \rightarrow$ state destruction	$k_q^{B^*}$	electronic quenching
$O_2 + B^* \rightarrow B^{**} + O_2$	$k_v^{O_2}$	VET
$M + B^* \rightarrow B^{**} + M$	k_v^M	VET
$O_2 + B^{**} \rightarrow$ state destruction	$k_q^{B^{**}}$	electronic quenching

background problems nor to risk the possibility of detecting the growth of other transition bands in the congested baseline. Moreover, the bands themselves are selected from the blue edge of the emission spectrum to avoid overlap with transitions ensuing from collisionally populated levels. For each position of the double monochromator, the signal is averaged to achieve reasonable precision of generally weak signals. A typical experiment involves collecting data from ~8−12 different sample compositions for building a single Stern−Volmer plot.

3. Results

3.1. Kinetic Mechanism. As reported in chemical timing papers,[18,19] changes in the S_1 pDFB fluorescence spectrum brought forth by high added pressures of O_2 can be described with a time-dependent picture. We use this concept for the kinetic mechanism in Table 1, which provides the framework for our chemical timing study of vibrational energy transfer (VET) from high vibrational levels.

Species B* in Table 1 is the initially pumped narrow S_1 vibrational energy domain. For the purposes of the chemical timing mechanism, it can be considered as a single state. Fluorescence from this state produces a spectrum with a discrete vibrational structure typical of a single state emission. Species B** represents the isoenergetic or nearby states in the S_1 vibrational manifold that are populated by either collisions or IVR. These levels produce broad unstructured fluorescence. Under collision-free conditions, B** emission dominates the spectrum because IVR is much faster than the radiative plus nonradiative S_1 decay. As added O_2 quenches the B* electronic state, the shortened time window for fluorescence reduces both the IVR decay of B* and the accompanying buildup of B**. Thus, emission in this short time window has a larger component from B*, and the B* vibrational bands become visible. Both B* and B** are destroyed by electronic state quenching with O_2. As explained below, these quenching rate constants differ. VET destruction of B* to form B** occurs via collisions with both O_2 and the added VET collision partner M.

The relative population of B^*, in the presence of a given O_2 pressure, during additions of the collision partner M is monitored by the intensity of the structured component of B* fluorescence. The intensities without and with the added M gas are designated I_0 and I_M, respectively. From the kinetic scheme in Table 1, one obtains the Stern−Volmer relationship:

$$\frac{I_0}{I_M} = 1 + \frac{k_v^M[M]}{k_f + k_{IVR} + (k_v^{O_2} + k_q^{B^*})[O_2]} \qquad (1)$$

The slope S of the Stern−Volmer plot of eq 1 can be simplified by ignoring the rate constant k_f because of its small size relative to other terms giving

$$S = \frac{k_v^M}{k_{IVR} + (k_v^{O_2} + k_q^{B^*})[O_2]} \qquad (2)$$

The desired rate constant k_v^M can be extracted from eq 2, provided that the three rate constants in the denominator are known. The value of the quenching rate constant $k_q^{B^*}$ by O_2 is available from previous total fluorescence measurements in our laboratory.[22] The constants k_{IVR} and $k_v^{O_2}$ for this level have not been directly measured.

A useful alternative representation of eq 2 is

$$\frac{1}{S} = \frac{k_{IVR}}{k_v^M} + \frac{(k_v^{O_2} + k_q^{B^*})[O_2]}{k_v^M} = \alpha + \beta[O_2] \qquad (3)$$

A plot of $1/S$ in the form of eq 3 for various O_2 pressures allows k_v^M to be determined from the observed β value without a need to know or assume a k_{IVR} value. Alternatively, k_v^M can be obtained from the observed α value without a need to know or assume a $k_v^{O_2}$ value.

A second experimental degree of freedom, as described in previous chemical timing papers,[17,18] is at our disposal. One can measure the intensity of the structured fluorescence component (I_S) relative to that of total emission (I_T) as a function of added O_2. With the assignment of I_S as B* emission and the assignment of I_T as B* + B** emission, simple relationships are derived from the mechanism.

$$I_S = \frac{\Omega}{k_f + k_{IVR} + (k_v^{O_2} + k_q^{B^*})[O_2]} \qquad (4a)$$

$$I_T = \frac{\Omega}{k_f + k_q^{B^{**}}[O_2]} \qquad (4b)$$

The experimental/instrumental constant Ω is eliminated by division of the two signals obtained under same experimental settings. The use of two distinct electronic quenching rate constants $k_q^{B^*}$ and $k_q^{B^{**}}$ is mandated by the electronic quenching mechanism proposed in a study of the quenching kinetics[22] (see below). Except for these distinct pDFB + O_2 interaction channels, the above expressions are consistent with the kinetic model used for the earlier chemical timing studies. If one ignores the rate constant k_f in the denominators of eq 4 because of its small size relative to other terms then from eq 4, one obtains an equation that casts I_T/I_S as a linear function of $1/[O_2]$:

$$\frac{I_T}{I_S} = \frac{k_v^{O_2} + k_q^{B^*}}{k_q^{B^{**}}} + \frac{k_{IVR}}{k_q^{B^{**}}}\left(\frac{1}{[O_2]}\right) \qquad (5)$$

3.2. Fluorescence Spectra and Quantitative Measurements. Figure 2 shows a pDFB absorption spectrum in which the absorption region providing access to $\epsilon_{vib} = 3700\ cm^{-1}$ is revealed as lying on the weak high-energy tail of the $S_1 \leftarrow S_0$ transition. We focus on this small feature and acquire a more detailed view in the segment of the fluorescence excitation spectrum shown in Figure 3. The pump laser is tuned to the

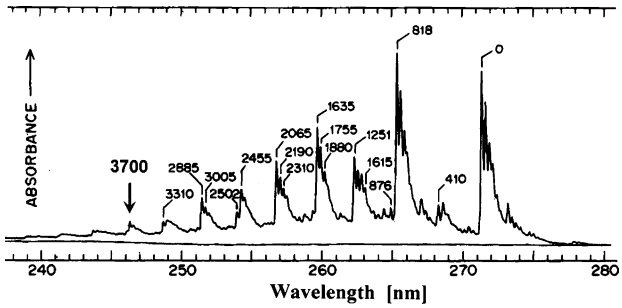

Figure 2. Low-resolution $S_1 \leftarrow S_0$ absorption spectrum of pDFB vapor indicating the absorption position leading to the $\epsilon_{vib} = 3700$ cm^{-1} level. (Adapted from ref 17.)

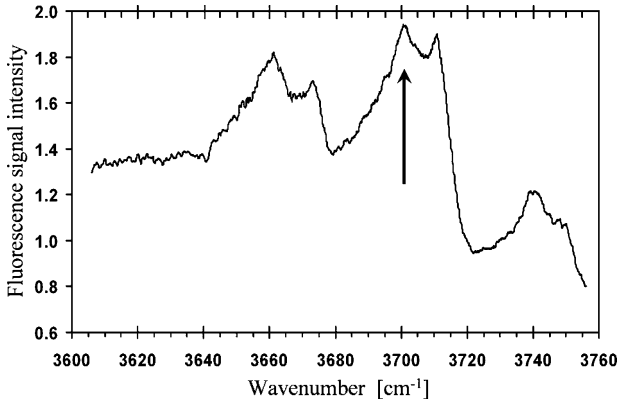

Figure 3. Fluorescence excitation spectrum of pDFB. The *x*-axis represents ϵ_{vib}, the wavenumber displacement of the pump position from the $S_1 \leftarrow S_0$ (0_0^0) origin at 36840 cm^{-1} (vacuum). The band maximum pumped for this study is indicated by the arrow.

indicated maximum to populate an S_1 vibrational region with nominal $\epsilon_{vib} = 3700$ cm^{-1}. The transition sits on an elevated baseline of congestion formed by many transitions with low oscillator strengths or by transitions with oscillator strengths distributed over many states. Band contours have tails to the red so that higher energy bands overlap this position. Although the nominal Franck−Condon transition is $3_0^1 5_0^3$ with a calculated position at 3705 cm^{-1} based on harmonic fundamentals, there is no way to check the transition assignments of the region. The laser pump bandwidth is 2 cm^{-1}. The maximum of the labeled weak feature corresponds to the laser position of approximately $0_0^0 + 3700$ cm^{-1}, and the laser is fixed at this position for all subsequent experiments.

As shown in Figure 1, the single vibronic level fluorescence (SVLF) spectrum from the $\epsilon_{vib} = 3700$ cm^{-1} level is broad and completely structureless. This congestion is a signature of extensive vibrational state mixing or IVR, and it is typical of fluorescence from high levels in general.

When sufficiently high pressures of O_2 are added to the pDFB sample, the spectrum undergoes a characteristic transformation as O_2 collisions create a narrow fluorescence time window. Figure 4 shows a series of normalized fluorescence spectra for O_2 pressures in the range of 1−16 kTorr acquired with 20 cm^{-1} resolution. Using the measured quenching rate constants,[22] the estimated fluorescence window is limited to only 10−100 ps for the pressure range of spectra in Figure 4. Similar spectra were previously acquired for many lower S_1 levels.[17,18] Gradual emergence of structure in response to rising O_2 pressure can be understood in terms of competition between IVR and electronic quenching by O_2. Although the total fluorescence intensity decreases substantially because of electronic quenching, the development of vibrational structure is our primary interest. The

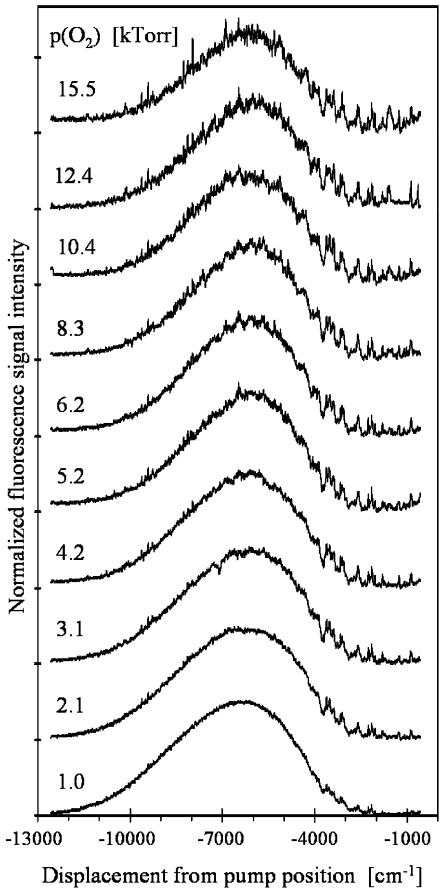

Figure 4. Normalized dispersed fluorescence spectra from S_1 pDFB with $\epsilon_{vib} = 3700$ cm^{-1} showing the effect of high O_2 pressures on the emission profile.

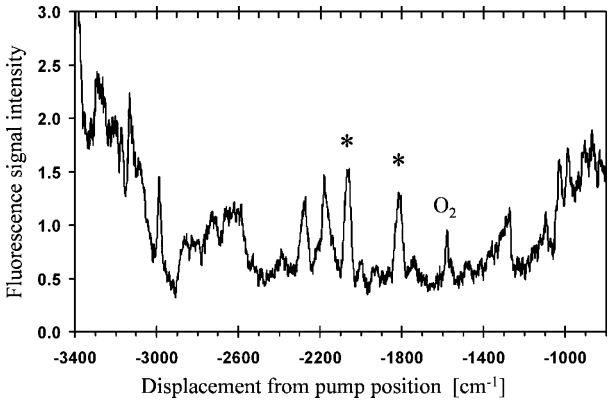

Figure 5. Short section of the dispersed fluorescence spectrum of pDFB with ~4 kTorr of O_2 displaying two marked bands (∗) that are monitored in the chemical timing−vibrational energy transfer (CT-VET) experiments. The selected transitions are conveniently located inside a 2000 cm^{-1} valley. The background intensity increases to the right because of the tail of scattered laser light, and to the left because of spectral congestion. The peak labeled "O_2" is due to O_2 Raman scattering.

structure enhancement ceases beyond about 10 kTorr, because of VET by O_2. In addition, the relative noise level becomes an increasing problem with the smaller fluorescence intensities. Thus, the compromise between IVR, electronic quenching, VET, and the signal/noise ratio restricts our optimal conditions for structure development to about 2−10 kTorr of O_2.

Figure 5 shows a segment of the SVLF spectrum of pDFB in about 4 kTorr of O_2. It displays several bands that can be

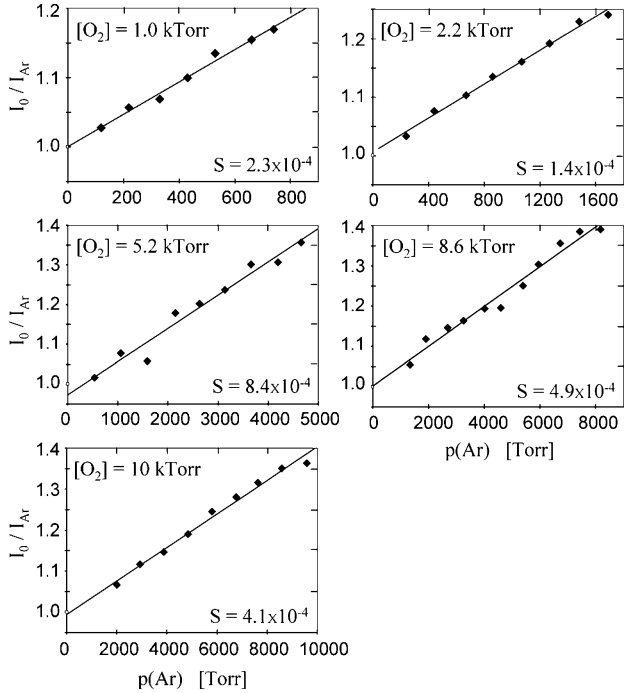

Figure 6. Five Stern−Volmer plots of the band intensities to investigate pDFB + Ar VET at different O_2 pressures. I_0 and I_{Ar} are signal intensities without and with added argon gas, respectively. The O_2 pressures and the slopes S of linear fits are indicated.

monitored in VET measurements. The two marked transitions are located in a valley about 2000 cm^{-1} wide between the tail of the laser pump at the blue end and the emission congestion at the red end. Consequently, these transitions are isolated and nearly free of interference from these two effects. The destination states of VET in pDFB collisions with Ar emit predominantly into a region below positions of the marked transitions without producing new structure inside the valley. In a CT-VET experiment, the intensities of the two marked bands are individually monitored, signal averaged, and combined at each argon pressure increment. No systematic difference between measurements of the two bands could be detected. The baseline intensity is subtracted from band intensities to yield the true band size and the relative structured fluorescence intensity that we are pursuing.

With the above procedure, we monitor the band intensity in response to increasing argon pressure at constant pDFB and O_2 pressures. Figure 6 shows five Stern−Volmer plots from these band measurements. The I_0/I_{Ar} axis represents the ratio of two signal intensities without and with added argon, respectively. O_2 pressures were fixed at one of five values between 1 and 10 kTorr to generate the five plots. In each experiment, the added argon pressures are large enough to generate a significant decrease in signal, but always below the O_2 pressure in order to guarantee that no S_1 pDFB molecule experiences more than a single Ar collision within its lifetime. The linear fit is constructed through typically 8−12 points. The plots are in the form of eq 1 with slopes given in the figures.

The set of spectra in Figure 4 also provides data for the IVR analysis. By separation of structure and congestion, it has been possible to obtain information about the IVR rate constant k_{IVR}.[17,18] Our separation procedure is based on an earlier understanding[19,23] that the congested component is a complex superposition of emission spectra from a very large number of B** states, the net product of which is a relatively simple, smooth curve similar to that of collision-free pDFB fluorescence

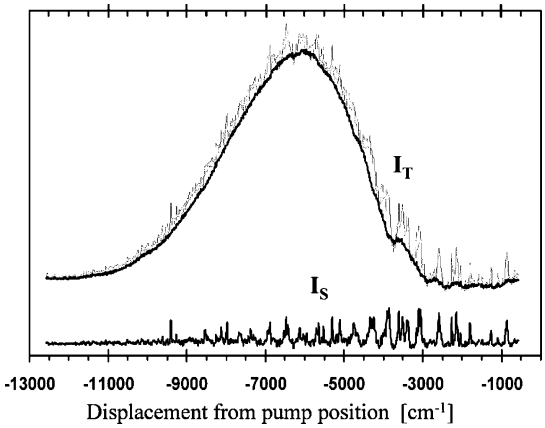

Figure 7. Dispersed fluorescence spectrum of pDFB with 6.2 kTorr O_2, showing the separation of the structured component (I_S) from the total fluorescence (I_T). The spectrum of the isolated structured component I_S is shown at the bottom.

in Figure 1. Structured features whose origin is the zero-order pumped B* state protrude from this bell-like curve.

It was demonstrated earlier[20] that O_2 addition indeed recovers fluorescence structure of the original zero-order pumped state. Using the example of emission with 6.2 kTorr of O_2, Figure 7 illustrates the separation of fluorescence intensity into its structured and unstructured components for quantitative IVR measurements. In the separation, we select any significant deviation from the smooth general baseline as the structured component. Our separation procedure is again based on the assumption that fully structured and fully unstructured emission spectra are simply additive so that the baseline of the structured spectrum can be delineated by interconnecting the bottoms of the valleys between groups of structures.

There are some concerns regarding the accuracy of the structured I_S versus total I_T fluorescence intensity measurements. For example, there is an O_2 Raman line at -1570 ± 10 cm^{-1} displacement from the pump position that becomes substantial relative to fluorescence at high O_2 pressures. This feature is removed before structure−congestion separation. The total fluorescence intensity from high-lying levels at high O_2 pressures is small, and the blank cell background becomes a significant artificial contribution to be subtracted from all measurements. Also, even after extensive signal averaging, there remains a certain degree of random noise that makes structure−congestion distinction imprecise. Finally, the quantitative results of structure−congestion separation also depend on the spectral resolution and on details of the separation procedure.

3.3. Rate-Constant Determination. The data provide two paths to determine the rate constant k_v^M, now specifically k_v^{Ar}, for our experiments with the collision partner Ar. Path A relies exclusively on the band intensity measurements I_0/I_M. Path B combines these data with additional measurements of the structured component I_S of fluorescence I_T/I_S.

3.3.1. Path A. The band intensities I_0/I_M are plotted in Figure 6 in the Stern−Volmer form, according to eq 1, for five different O_2 pressures. In principle, k_v^{Ar} could be obtained from the slope S of any one plot in Figure 6, provided the rate constants in the denominator of eq 2 are all known. Among these, k_{IVR} and $k_v^{O_2}$ are problems. One way to reduce the problem is provided by the series of I_0/I_M measurements at various fixed O_2 pressures.

Equation 3 predicts that the reciprocal slopes $1/S$ of these plots should be a linear function of the O_2 pressure. Figure 8 contains this plot, from which it is seen that the predicted relationship $1/S = \alpha + \beta[O_2] = 1890 + 2.13[O_2]$ is well obeyed.

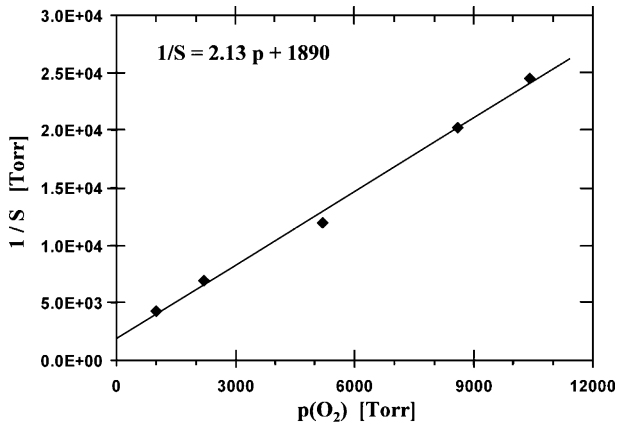

Figure 8. Inverse Stern−Volmer slopes (1/*S*) from Figure 6, as a function of the O_2 pressure, according to eq 3.

From the slope,

$$k_v^{Ar} = \frac{k_v^{O_2} + k_q^{B^*}}{\beta} = \frac{k_v^{O_2} + k_q^{B^*}}{2.13} \tag{6}$$

one can determine k_v^{Ar} without any knowledge of k_{IVR}. From the intercept,

$$k_v^{Ar} = \frac{k_{IVR}}{\alpha} = \frac{k_{IVR}}{1890} \tag{7}$$

one can determine k_v^{Ar} without any knowledge of $k_v^{O_2}$. Both rate constants needed to determine k_v^{Ar} from eq 6 are known, whereas k_{IVR}, which is needed for eq 7, must come from additional sources.

For use of eq 6, we first consider the electronic quenching rate constant $k_q^{B^*}$. Our earlier study[22] of O_2 fluorescence quenching kinetics revealed that two channels participate in the electronic state destruction of S_1 pDFB. One is a reversible channel involving a product, possibly a pDFB•O_2 charge-transfer complex, that can reform S_1 pDFB on a second O_2 collision. The other is an irreversible channel whose product may be a triplet state. Accordingly, two rate constants are associated with electronic destruction of the S_1 state. Since they differ by about an order of magnitude, it is important to choose the correct value for the present kinetic analysis.

In the low pressure limit, where the reversibility disappears from the O_2 quenching kinetics, the observed effective quenching rate constant $k_q^{B^*}$ is the sum of the rate constants for the two channels. Ironically, it is this limiting low pressure value that is appropriate for B* destruction at the high O_2 pressures of our present experiments. One can see why by considering the large number of B** states versus the single B* state. Although the reversible quenching kinetics is fully operative at our high O_2 pressures, it is overwhelmingly probable that the product of the reversible step is the surrounding S_1 vibrational B** field and not B* itself. Therefore, the destruction of B* by O_2 electronic quenching is a one-way process.

Table 2 shows two sets of data for the electronic quenching rate constants. One set refers to measurements made specifically at $\epsilon_{vib} = 3700$ cm^{-1}. These values are based on the assumption that $\tau_f = 5.1$ ns, which is an extrapolation of measured fluorescence lifetimes[24] from 18 states with $\epsilon_{vib} \leq 3310$ cm^{-1}. The other set refers to an average of k_q values obtained for several S_1 states for which the fluorescence lifetimes are known. We can use this average because it has been found that quenching rate constants are independent of the vibrational level.

TABLE 2: S_1 PDFB + O_2 Electronic Quenching Rate Constants

rate constant	for $\epsilon_{vib} = 3700$ cm^{-1}[a]	average over states[b]
$k_q^{B^*}$ (10^6 Torr^{-1} s^{-1})	10	8.0
$k_q^{B^{**}}$ (10^6 Torr^{-1} s^{-1})	0.90	0.99

[a] From ref 22. [b] To be published.

There are two independent estimates of $k_v^{O_2}$ for use with eq 6. One is derived from the state-to-field $k_v^{O_2}$ rate constants that have been directly measured[25] for numerous S_1 pDFB levels with $\epsilon_{vib} < 2500$ cm^{-1}. The rate constants increase gradually with ϵ_{vib}, and extrapolation to $\epsilon_{vib} = 3700$ cm^{-1} yields $k_v^{O_2} \approx 10.8 \times 10^6$ Torr^{-1} s^{-1}.

The other estimate uses the approximation that $k_v^{Ar} = k_v^{O_2}$. This estimate is derived from a relationship[26] correlating k_v^M values for many collision partners that cause state-to-field VET in S_1 benzene[27] with $\epsilon_{vib} \approx 2000$ cm^{-1}. Although the oxygen VET rate constant in those studies was obscured by an electronic state quenching channel that was not separable from VET, the good representation of the data for more than 20 collision partners suggests that O_2 would also fit the relationship.

The relationship is based on correlating collision cross-sections with the intermolecular well-depths between collision partners. The predicted relationship

$$\sigma = C \exp\left(\frac{\sqrt{\epsilon_{MM}\epsilon_{B^*B^*}}}{k_B T}\right) \tag{8}$$

has been shown to be reasonably good for many types of collisional processes.[26] In this expression, σ is the cross section between the target B* and the collision partner M, ϵ_{MM} is the intermolecular potential well depth for the M−M pair, and $\epsilon_{B^*B^*}$ is the intermolecular potential well depth for the B*−B* pair. The proportionality constant C is characteristic of the target species and the process under discussion. We focus on data for the same target B* with various M partners so that the constant C is obviously independent of the M gas. The only parameter that makes the cross-section different from one M partner to another is ϵ_{MM}. The parameter C, the temperature T, and the well-depth $\epsilon_{B^*B^*}$ generate a common constant in eq 8; therefore, the rate constants for two M partners can be related by $k_{O_2}/k_{Ar} \approx \sigma_{O_2}/\sigma_{Ar} = \exp[(\sqrt{\epsilon_{O_2-O_2}} - \sqrt{\epsilon_{Ar-Ar}})\sqrt{\epsilon_{B^*-B^*}}/(k_B T)] \approx 1$. This result comes from the parameter $\sqrt{\epsilon_{MM}}/k_B$, which has values of 11.0 K$^{1/2}$ and 10.8 K$^{1/2}$ for argon and O_2, respectively.[26] The close match in well-depths predicts that the VET rate constants with argon and O_2 should be almost the same. From the $k_v^{Ar} = k_v^{O_2}$ approximation with eq 6, one obtains $k_v^{Ar} = k_q^{B^*}/(\beta - 1) = k_q^{B^*}/1.13$.

3.3.2. Path B. This path to determination of k_v^{Ar} makes use of the measurements of I_T/I_S concerning the fraction of emission contributed by the structured component. When these data are combined with the band intensity measurements I_0/I_M used previously for path A, one can determine the value of k_v^{Ar} without using any assumed rate constant values. As a bonus, one also obtains $k_v^{O_2}$ and k_{IVR} directly.

The I_T/I_S measurements are interpreted by eq 5 with two rate constants ($k_q^{B^*}$ and $k_q^{B^{**}}$) for O_2 fluorescence quenching. As explained in the path A discussion, $k_q^{B^*}$ is the limiting value for quenching at low pressures when the reversible kinetics of the quenching is precluded. In contrast, the quenching of B** under our high O_2 pressure conditions corresponds to the high pressure

TABLE 3: Rate Constants for S_1 pDFB

	source[a]			
rate constant	path A with $k_v^{O_2} = 10.8 \times 10^6$ Torr^{-1}s^{-1}	path A with $k_v^{O_2} = k_v^{Ar}$	path B via eq 6	path B via eq 7
k_v^{Ar} (10^6 Torr^{-1} s^{-1})[b]	9.8 (8.8)	8.8 (7.1)	8.6 (9.4)	11 (12)
$k_v^{O_2}$ (10^6 Torr^{-1} s^{-1})[b]			8.3 (12)[c]	
k_{IVR} (10^{10} s^{-1})	1.9 (1.7)[d]	1.7 (1.3)[d]	2.0 (2.2)[e]	
τ_{IVR} (ps)	54 (60)[f]	60 (75)[f]	49 (45)[f]	

[a] Values without parentheses are derived with quenching parameters specifically obtained for $\epsilon_{vib} = 3700$ cm^{-1} whereas those within the parentheses refer to use of the average of quenching parameters over several vibrational states. [b] For conversion to cm^3 molecule^{-1} s^{-1}, multiply by 3.1×10^{-17}. [c] From eq 10. [d] From eq 7 with the corresponding k_v^{Ar} value. [e] From eq 2. [f] $\tau_{IVR} = k_{IVR}^{-1}$.

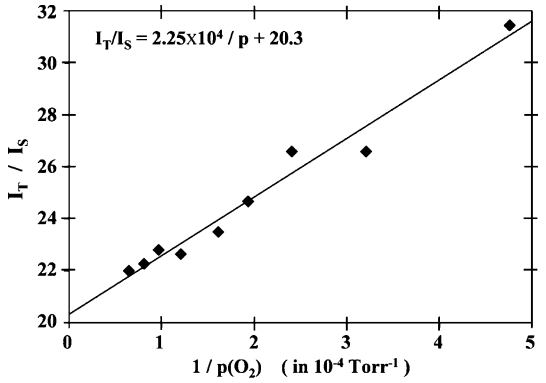

Figure 9. Ratio of total to structured fluorescence intensity (I_T/I_S) as a function of the inverse O_2 pressure, according to eq 5.

limit where the reversible kinetics is in full operation. The observed quenching rate constant in this limit is that for the irreversible channel alone. As seen in Table 2, it is approximately an order of magnitude smaller than k_q^{B*}.

Figure 9 shows a plot of I_T/I_S as a function of $1/[O_2]$ according to eq 5 of the kinetic mechanism. The predicted linear relationship is reasonably well obeyed with

$$\frac{I_T}{I_S} = 20.3 + \frac{22500}{[O_2]} \tag{9}$$

$k_v^{O_2}$ can be derived from the intercept using eq 5:

$$20.3 = \frac{k_v^{O_2} + k_q^{B^*}}{k_q^{B^{**}}} \tag{10}$$

k_{IVR} can be derived from the slope using eq 5:

$$22500 = \frac{k_{IVR}}{k_q^{B^{**}}} \tag{11}$$

With $k_v^{O_2}$ and k_{IVR} now provided by the I_T/I_S measurements, k_v^{Ar} can be determined from both eqs 6 and 7.

Table 3 lists the rate constants obtained by these procedures. A matrix of k_v^{Ar} values is provided by paths A and B with two sources of $k_v^{O_2}$ and with two sets of electronic quenching rate constants.

As described previously, the IVR rate constant can be derived directly from the path B data analysis, using eq 11. In addition, k_{IVR} can also be obtained by back tracking along the path A analysis where the path A values of k_v^{Ar} are used with eq 7. The results in Table 3 show that the various k_{IVR} values for a given set of quenching parameters lie within ~10% of their average. This degree of consistency between the path A and path B values is a source of confidence in the data and their analyses.

Another internal consistency check is provided by comparing a slope-to-intercept ratio derived from I_T/I_S measurements (Figure 9) with the intercept-to-slope ratio of $1/S$ data derived from I_0/I_M measurements (Figure 8). Both values should be $k_{IVR}/(k_v^{O_2} + k_q^{B*})$ according to eqs 3 and 5. The observed ratios 1890 Torr/2.13 = 890 and 22 500 Torr/20.3 = 1100 Torr from Figures 8 and 9, respectively, are within 20% of each other.

In our analysis, we have obtained eqs 3 and 5 by ignoring the collision-free fluorescence rate constant k_f in their respective predecessors, eqs 1 and 4. With the assumption that our extrapolation of k_f values from lower levels to obtain $\tau_f = 5.1$ ns for $\epsilon_{vib} = 3700$ cm^{-1} is accurate, k_f is indeed sufficiently small to be neglected relative to the IVR rate and relative to the rates of collisional destruction channels which are all tuned by adjusting [Ar] and [O_2] to compete favorably with IVR. However, if the k_f extrapolation is an underestimate, then it would significantly contribute to the error in all our rate constant values. In particular, an underestimate of k_f would lead to an underestimate of both electronic quenching k_q and VET k_v parameters. An indication that k_f is not substantial relative to k_{IVR} is that the observed trend in Figure 9 is strongly linear. With $k_f \approx 0.1k_{IVR}$, the trend would be nonlinear with a slow drift upward, and with $k_f \approx k_{IVR}$, the trend would be decreasing.

4. Discussion

The principal measurements of this work concern the absolute rate constant k_v^{Ar} for state-to-field VET by Ar in collision with S_1 pDFB pumped to $\epsilon_{vib} = 3700$ cm^{-1}. Eight values of k_v^{Ar} are displayed in Table 3. They arise in part from using alternative paths to the derived values and in part from using different choices for the electronic quenching rate constant and the constant $k_v^{O_2}$ needed in the calculation. Because the spread of values is reasonably small, the derived rate constants obviously do not have strong sensitivity to the method of derivation or to the small variations in rate constants used in the derivation. It is not possible to choose one as a single preferred value. Accordingly, we adopt as the preferred value the average $k_v^{Ar} = (9.4 \pm 1.5) \times 10^6$ Torr^{-1} s^{-1}, where the 16% uncertainty is the standard deviation from the mean.

Each k_v^{Ar} value is associated with some unique uncertainty. Path A, with $k_v^{O_2} = 10.8 \times 10^6$ Torr^{-1} s^{-1}, is based on the assumption that $k_v^{O_2}$ may be extrapolated from the trend of VET rate constants increasing with ϵ_{vib} for lower-lying states. Path A with $k_v^{O_2} = k_v^{Ar}$ is based on the assumption that the generally obeyed correlation of eq 8 holds for this system. The path B values are based on the absence of systematic error in the procedure for structured−unstructured fluorescence separation.

The reasonably close agreement among the four pairs of values suggests that these assumptions and procedures are acceptable. However, an overriding assumption that involves a potentially large systematic error still remains. Is the derived VET rate constant free of substantial perturbation by the large O_2 pressures used to obtain it? The question has been explored by an explicit series of experiments on an S_1 pDFB level with $\epsilon_{vib} = 818$ cm^{-1} for which the state-to-field VET rate constant for Ar is securely known from measurements in the standard manner without added O_2. Past oxygen-free measurements for this level have given $k_v^{Ar} = 3.3 \times 10^6$ Torr^{-1} s^{-1},[13] 3.5×10^6 Torr^{-1} s^{-1},[28] and 4.0×10^6 Torr^{-1} s^{-1}.[12] Measurements[28] in the presence of O_2 at ~1000−7000 Torr showed no trend with increasing O_2 additions and an average rate constant of $k_v^{Ar} = 3.9 \times 10^6$ Torr^{-1} s^{-1}. This value is within the range of the oxygen-free measurements. Thus, by this test, perturbation of the rate constant by large additions of O_2 (in the kTorr range) is undetectable.

Use of the S_1 rate constant k_v^{Ar} in discussions of the activation/deactivation processes in thermal unimolecular reactions requires that questions of reliability be expanded to a larger issue. What are the consequences of working with an excited electronic state as opposed to the electronic ground states that pertain to almost all thermal unimolecular activation/deactivation studies? The issue is explored by an approach analogous to that used for exploring oxygen effects on the rate constant. With stimulated emission pumping experiments by Kable, Thoman, and Knight,[29] explicit comparisons of VET in S_1 and S_0 pDFB are available. As discussed elsewhere,[13] the S_1 and S_0 rate constants for regions of comparable state densities never differ by more than a factor of 2 and, in some regions, are much closer.

4.1. The IVR Rate Constant. The IVR lifetimes in the range of 45−75 ps as listed in Table 3 have been obtained as a byproduct of these experiments. The combined uncertainties are difficult to assess and the use of the term "estimate" for k_{IVR} is probably appropriate. For this reason, it is difficult to know whether the lifetimes are actually longer than the 16−36 ps ranges for four lower S_1 pDFB levels with 2455 cm$^{-1} \leq \epsilon_{vib} \leq$ 3310 cm^{-1}, as determined by a chemical timing study.[17] That study used a so-called statistical case analysis that closely replicates the path B method of the present study.

Previous chemical timing experiments[17] give additional $k_v^{O_2}$ values for initial levels with 1500 cm^{-1} < ϵ_{vib} < 3300 cm^{-1}. The individual $k_v^{O_2}$ values vary significantly with no trend and a mean $k_v^{O_2}$ value of 5.4×10^6 Torr^{-1} s^{-1}. This is likely an underestimate, because it is significantly below the values of direct $k_v^{O_2}$ measurements from similar levels and also is significantly below our values for $\epsilon_{vib} = 3700$ cm^{-1}. A likely cause of this deviation is the use of different electronic quenching parameters. We operate with two k_q constants of ~0.9×10^6 and ~9×10^6 Torr^{-1} s^{-1} as opposed to a single k_q constant with 4.24×10^6 Torr^{-1} s^{-1} used in the chemical timing experiments.[17] Otherwise, the kinetic models are the same. If we use the $k_v^{O_2} = 5.4 \times 10^6$ Torr^{-1} s^{-1} value as a lower extreme in eq 6, a value $k_v^{Ar} = 7 \times 10^6$ Torr^{-1} s^{-1} would be observed.

4.2. Comparisons with the Lennard-Jones Rate Constant. The state-to-field VET benchmark used for modeling the activation/deactivation processes in thermal unimolecular reactions is the rate constant for the collision pair operating with a Lennard-Jones intermolecular potential. For Ar in collision with pDFB, the constant[29] is $k_{LJ}^{Ar} = 17.5 \times 10^6$ Torr^{-1} s^{-1}. When compared with the value $k_v^{Ar} = 9.4 \times 10^6$ Torr^{-1} found in the present study, it is seen that the state-to-field VET efficiency for $\epsilon_{vib} = 3700$ cm^{-1} is only about half of the benchmark Lennard-Jones assumption.

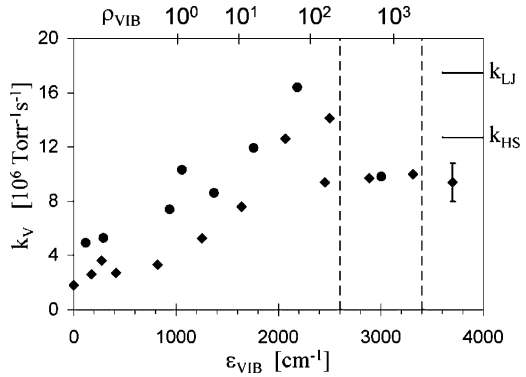

Figure 10. Plot of the measured values of k_v^{Ar} against the energy ϵ_{vib} and the state density ρ_{vib} of the pumped level for state-to-field VET of S_1 pDFB by Ar. Markers for the hard sphere and the Lennard-Jones rate constant values are shown to the right. The dashed line near 2600 cm^{-1} indicates the highest energy region used in the first study (ref 12). The dashed line near 3400 cm^{-1} indicates the high energy limit for determining rate constants in the standard manner without added O_2. The "error bar" on the $\epsilon_{vib} = 3700$ cm^{-1} value represents the extrema of values in Table 3. Pumped levels containing a quanta of v'_{30} are indicated by solid circles.

Given this result, we explore the possible relevance to the activation/deactivation problem. One issue concerns how the states at $\epsilon_{vib} = 3700$ cm^{-1} replicate two characteristics central to the high vibrational region of activated molecule. In this region, the state densities are so high that the states overlap to form a quasi-continuum, and the vibrational states are so highly mixed in a zero-order harmonic basis that none is dominated by a single state zero-order description. Both conditions are well established for S_1 pDFB with $\epsilon_{vib} = 3700$ cm^{-1}. The completely unstructured fluorescence from the pumped state is a secure indication of their highly mixed character. The state density $\rho_{vib} \approx 4000$ per cm^{-1} gives a level spacing of only about 3×10^{-4} cm^{-1}, which is much smaller than the level width of about 10^{-2} cm^{-1} established by the collision-free S_1 lifetime of a few nanoseconds.

The plot of rate constants in Figure 10 places the k_v^{Ar} value for $\epsilon_{vib} = 3700$ cm^{-1} in the context of values for the lower levels. The plot has three energy domains. The rate constants for ϵ_{vib} < 2600 cm^{-1} have a strong dependence on the initial quantum state identity.[12,13] Modeling has had partial success in describing this sensitivity, with the demonstration that the quantum state sensitivity is largely due to specific state-to-state channels that are specially favored from some initial quantum states.[12] The modeling also shows that the trend to larger VET rate constants with increasing ϵ_{vib} occurs because of contributions from more state-to-state channels at higher energies, each with a small transition probability.[12,14]

The next initial energy domain in Figure 10, with 2887 cm$^{-1} \leq \epsilon_{vib} \leq$ 3310 cm^{-1}, is the highest for the rate constants that can be measured without added O_2. It has been argued[13] that the VET rate constant sensitivity to initial quantum states must eventually dampen out as the extensive state mixing of higher levels severely dilutes any individual quantum state identities. In addition, it was also argued that the upward drift as higher initial levels are pumped must eventually stop. There is, however, little information about where this happens or whether the rate constants level off or perhaps even begin a decline with increasing vibrational energy. The three constants in this domain suggestively display the expected characteristics of the high

levels previously described. In the midst of a sensitive test for quantum state sensitivity,[13] they show none and with equal values to within the measurement uncertainty, they also seem to have no significant response to increasing initial vibrational energy.

The third energy domain, with $\epsilon_{vib} > 3500$ cm^{-1}, concerns regions for which our new method with high O_2 pressures must be used. It has only one value so far, namely that for $\epsilon_{vib} = 3700$ cm^{-1} of the present study. The value is approximately the same as that for the three rate constants in the second domain. It continues the suggestive trend of those rate constants in that they respond neither to quantum state identities nor to increasing ϵ_{vib}.

Whether the rate constants have leveled off, as one scenario proposes for high ϵ_{vib} rate constants, remains to be seen when data from higher energies become available. The emerging pattern of rate constants does show, however, that the Lennard-Jones benchmark remains a factor of 2 above the rate constants for the highest levels seen thus far in the S_1 pDFB + Ar system. For reasons not understood, the rate constants for these highest levels are, in fact, well below some for lower levels where strong quantum state sensitivity exists.

5. Conclusions

A method has been developed to measure the absolute rate constant for state-to-field vibrational energy transfer (VET) involving a high region of the S_1 *p*-difluorobenzene (pDFB) vibrational manifold, where the states form a quasi-continuum. In this region, the standard approach based on observations of vibrational band intensities in $S_1 \rightarrow S_0$ fluorescence after pumping a selected S_1 level is precluded because the fluorescence is without any vibrational structure. The new method is a variant of the so-called chemical timing (CT) approach used for study of intramolecular vibrational redistribution (IVR), whereby a high pressure of O_2 is used to induce vibrational structure in the otherwise structureless fluorescence spectrum.

The CT-VET method is applied to the $\epsilon_{vib} = 3700$ cm^{-1} level of S_1 pDFB in collision with Ar. Vibrational band intensity measurements during the additions of argon gas to a mixture of 4 Torr of pDFB and a fixed O_2 pressure in the range of 1000−10 000 Torr yield good Stern−Volmer plots. The VET rate constant extracted from these plots varies slightly according to the method of analysis and choices among values of other rate constants needed for the determination. The preferred value of the rate constant is $k_v^{Ar} = (9.4 \pm 1.5) \times 10^6$ Torr^{-1} s^{-1}, with the uncertainty being the standard deviation of the eight values contributing to the mean.

This rate constant pertains to a region of the vibrational manifold that is not only a quasi-continuum but also a region of highly mixed states. These characteristics are the hallmarks of the vibrational manifold of vibrationally hot molecules in thermal unimolecular reactions. In the absence of measurements, VET rate constants for these regions are usually assumed to be those of Lennard-Jones elastic collisions. Our observed k_v^{Ar} rate constant for $\epsilon_{vib} = 3700$ cm^{-1} is only about half of the Lennard-Jones benchmark.

This rate constant is the most recent of a series of measurements for the S_1 pDFB + Ar system at higher and higher vibrational energies. Its value is within the experimental uncertainty of those for the 2888 cm$^{-1} \leq \epsilon_{vib} \leq 3310$ cm^{-1} region. This result suggests that the VET rate constants observed for the highest energy regions of our studies might be approaching a limiting value characteristic of molecules with chemically significant initial vibrational energies. Further experiments are in progress to test this proposition.

Acknowledgment. We are grateful for the financial support of the National Science Foundation. The preliminary explorations of the CT-VET method by Dr. Todd A. Stone have been most helpful.

References and Notes

(1) Barker, J. R.; Toselli, B. M. *Int. Rev. Phys. Chem.* **1993**, *12*, 305.
(2) Oref, I.; Tardy, D. C. *Chem. Rev.* **1990**, *90*, 1407.
(3) Weston, R. E.; Flynn, G. W. *Annu. Rev. Phys. Chem.* **1992**, *43*, 559.
(4) Xue, B.; Han, J.; Dai, H. L. *Phys. Rev. Lett.* **2000**, *84*, 2606.
(5) Zhang, M.; Han, J.; Liu, P.; Muller, D.; Dai, H.-L. *J. Phys. Chem. A* **2003**, *107*, 10845.
(6) Park, J.; Lawrence, S.; Lemoff, A. S.; Werner, K.; Mullin, A. S. *J. Chem. Phys.* **2002**, *117*, 5221.
(7) Goos, E.; Hippler, H.; Kachiani, C.; Svedung, H. *Phys. Chem. Chem. Phys.* **2002**, *4*, 4372.
(8) Seiser, N.; Kavita, K.; Flynn, G. W. *J. Phys. Chem. A* **2003**, *107*, 8191.
(9) Kappel, C.; Luther, K.; Troe, J. *Phys. Chem. Chem. Phys.* **2002**, *4*, 4392.
(10) Abel, B.; Lange, N.; Reiche, F.; Troe, J. *J. Chem. Phys.* **1999**, *110*, 1404.
(11) Barker, J. R.; Ortiz, N. F. *Int. J. Chem. Kinet.* **2001**, *33*, 246.
(12) Catlett, D. L.; Parmenter, C. S.; Pursell, C. J. *J. Phys. Chem.* **1995**, *99*, 7371.
(13) Stone, T. A.; Parmenter, C. S. *J. Phys. Chem. A* **2002**, *106*, 938.
(14) Tang, K. Y.; Parmenter, C. S. *J. Chem. Phys.* **1983**, *78*, 3922.
(15) Timbers, P. J.; Parmenter, C. S.; Moss, D. B. *J. Chem. Phys.* **1994**, *100*, 1028.
(16) Longfellow, R. J.; Moss, D. B.; Parmenter, C. S. *J. Phys. Chem.* **1988**, *92*, 5438.
(17) Holtzclaw, K. W.; Parmenter, C. S. *J. Chem. Phys.* **1986**, *84*, 1099.
(18) Coveleskie, R. A.; Dolson, D. A.; Parmenter, C. S. *J. Phys. Chem.* **1985**, *89*, 655.
(19) Coveleskie, R. A.; Dolson, D. A.; Parmenter, C. S. *J. Phys. Chem.* **1985**, *89*, 645.
(20) Holtzclaw, K. W.; Parmenter, C. S. *J. Phys. Chem.* **1984**, *88*, 3182.
(21) Dolson, D. A.; Parmenter, C. S.; Stone, B. M. *Chem. Phys. Lett.* **1981**, *81*, 360.
(22) Tasic, U. S.; Davidson, E. R.; Parmenter, C. S. *J. Phys. Chem. A* **2003**, *107*, 3552.
(23) Dolson, D. A.; Holtzclaw, K. W.; Moss, D. B.; Parmenter, C. S. *J. Chem. Phys.* **1986**, *84*, 1119.
(24) Guttman, C.; Rice, S. A. *J. Chem. Phys.* **1974**, *61*, 661.
(25) Catlett, D. L., Jr. Vibrational Energy Flow in the S_1 ($^1B_{2u}$) State of *p*-Difluorobenzene. Ph.D. Thesis, Indiana University, Bloomington, IN, 1985.
(26) Lin, H. M.; Seaver, M.; Tang, K.; Knight, A. E. W.; Parmenter, C. S. *J. Chem. Phys.* **1979**, *70*, 5442.
(27) Logan, L. M.; Buduls, I.; Knight, A. E. W.; Ross, I. G. *J. Chem. Phys.* **1980**, *72*, 5667.
(28) Tasic, U. S.; Parmenter, C. S., to be published.
(29) Kable, S. H.; Thoman, J. W.; Knight, A. E. W. *J. Chem. Phys.* **1988**, *88*, 4748.